Giant Diffusion of Nanomechanical Rotors in a Tilted Washboard Potential

L. Bellando,[*] M. Kleine, Y. Amarouchene,[†] M. Perrin,[‡] and Y. Louyer[§]

Université de Bordeaux, CNRS, LOMA, UMR 5798, F-33405 Talence, France

We present an experimental realization of a biased optical periodic potential in the low friction limit. The noise-induced bistability between locked (torsional) and running (spinning) states in the rotational motion of a nanodumbbell is driven by an elliptically polarized light beam tilting the angular potential. By varying the gas pressure around the point of maximum intermittency, the rotational effective diffusion coefficient increases by more than 3 orders of magnitude over free-space diffusion. These experimental results are in agreement with a simple two-state model that is derived from the Langevin equation through using timescale separation. Our work provides a new experimental platform to study the weak thermal noise limit for diffusion in this system.

Thermal diffusion in a tilted periodic (also named washboard) potential constitutes an archetypal model of transport phenomena in nonequilibrium statistical physics [1,2]. It describes a diverse range of systems, including Josephson junctions [3], molecular motors [4], synchronization phenomena [5], and diffusion on crystal surfaces [6], to name only a few.

Brownian particles moving in the tilted potential at nonzero temperature exhibit two distinct well-characterized limiting behaviors: locked and running states. The first emerges when the potential wells are deeper than the thermal energy scale, the diffusing particle remains in a local minimum. In the latter, a sufficient tilt of the potential, lowering its energy barrier, allows the particle to flow down the potential wells. Depending on the system parameters (friction, temperature, and tilt), both solutions may coexist, and stochastic transitions between locked and running states may occur. It has been shown, both experimentally [4,7,8] and theoretically [9,10], that in this two-state coexistence regime, the effective diffusion coefficient can be enhanced by several orders of magnitude relative to the free diffusion coefficient. However, this has only been experimentally observed in the overdamped regime which is by now a fully understood stochastic process [2].

To our knowledge, an experimental study of giant diffusion in the strongly inertial (underdamped) regime is still missing. The theoretical problem is also more demanding in the underdamped and weak noise limits because the usual expansion of the matrix continued fraction [2] fails to converge well [11]. On these grounds, this nonlinear stochastic system in the low-noise and low-damping limits is still attractive [11].

We propose a simple experimental setup based on the optical trapping of a nanodumbbell in a moderate vacuum. A special feature of our experiment is that the friction coefficient, being linearly proportional to the gas pressure

P, can be tuned over several orders of magnitude. Therefore, for a nearly constant temperature, Brownian motion can move from the overdamped to the underdamped regime. This makes the optical trapping setup a suitable platform to study stochastic dynamics in the low-friction regime [12–14].

The main focus of this Letter is the analysis of the rotational diffusivity in the bistability region for an underdamped stochastic mechanical nanorotor traveling in a tilted periodic potential. We provide experimental confirmation of a giant diffusivity by tracking the rotational motion of a single silica nanodimer. Because of the experimentally achieved timescale separation, we show that the effective diffusion is well described by a two-state model for this nearly one-dimensional rotational motion.

The experimental setup consists of a vacuum optical tweezer trapping a dielectric silica dumbbell made of two nanospheres of nominal radius 68 ± 7 nm [15,16]. The continuous wave trapping laser beam (wavelength, $\lambda = 1064$ nm and power, 180 mW) passes through an objective lens with a 0.8 numerical aperture, the polarization's ellipticity of which can be changed by a quarter-wave plate. A detailed description of the experimental setup, calibration, and processing procedures is given in the Supplemental Material [17] including Refs. [18–32]. The shape and the size of the dimer are assessed under linear polarization, and correspond to an aspect ratio $L/D = 1.8$, with two spheres of radius $R_p = 65.7$ nm, where $D = 2R_p$ and L is the major axis length of the dimer. Our detection system is able to simultaneously record the particle's center of mass motion and its angular displacement.

The nanodimer experiences both a trapping force and a torque, both of which are induced by elliptically polarized light. In particular, when such an asymmetric Rayleigh scatterer lies in the transverse $(\hat{x}, \hat{y})$ plane, corresponding to $\theta = \pi/2$, the torque reads

$$M = M_C - M_L \sin(2\varphi), \qquad (1)$$

where φ is the angle between the dimer main axis and the lab's horizontal $\hat{x}$ axis. Its time evolution is related to the dimer rotation around the $\hat{z}$ optical axis. M_C and M_L are respectively the *circular* and *linear* contributions of the optical torque which depend on the dimer polarizability tensor and the laser beam polarization [17].

In a linearly polarized optical tweezer, where $M_C = 0$, the long axis of the dimer (i.e., in the direction of greatest polarizability) will tend to align with the laser beam polarization. This is because the polarizability of the dimer along its long axis is greater than the polarizability perpendicular to it. As a result, the dimer acts as a torsion balance with a linear restoring torque, $-2M_L\varphi$. The libration pulsation Ω_L is well approximated in the low friction limit $(\Gamma_\varphi \ll \Omega_L)$ by $\sqrt{2M_L/I_z}$, where $I_\perp$ is the moment of inertia.

In contrast, for a circularly polarized trap, where $M_L = 0$, the asymmetric particle undergoes a constant torque, whatever its orientation φ. As a result of the continuous transfer of angular momentum, the particle will spin about the $\hat{z}$ axis at constant frequency, as given by $\Omega_R = M_C/I_\perp\Gamma_\varphi$, where Γ_φ is the rotation or torsional vibration damping rate about the $\hat{z}$ optical axis (see Ref. [17] for its determination). Note that the rotation frequency can exceed GHz, which allows us to study material stresses due to centrifugal forces [33,34], measure ultraweak torques [35,36], and examine quantum features of rotation [37,38].

Figure 1(a) illustrates the potential landscape and orientational dynamics for different polarization states. Considering the general case, for elliptical polarization, the potential has a washboard shape: $U(\varphi) = M_L\sin^2(\varphi) - M_C\varphi$, and one can observe running and locked states. Below, we only consider elliptical polarization which is held constant at $\phi_{\lambda/4} = 25°$, the angle of the quarter-wave plate.

The dynamics of an asymmetric Brownian particle trapped under elliptically polarized light is six dimensional with translational and rotational degrees of freedom coupled to each other. This generally leads to a highly nonlinear problem [36,39,40]. However, in the following, we show that the giant diffusion phenomenon is well described by one-dimensional rotational dynamics. Comparison between the experiment and numerical simulations is made quantitative provided that an additional term is added to the usual *extinction* optical torque ($\propto \Re[\mathbf{p} \times \mathbf{E}_{\text{inj}}]$, with $\mathbf{p}$ the dipole moment and $\mathbf{E}_{\text{inj}}$ the incident electric field). This extra term, called *scattering* torque ($\propto \Im[\mathbf{p} \times \mathbf{p}^*]$), is due to the interference of the fields scattered by the particle [17,41]. This φ angle dynamics reproducing the stochastic jumps between torsion and continuous rotation states is described by the Langevin equation

$$I_\perp\ddot{\varphi} = -I_\perp\Gamma_\varphi\dot{\varphi} + M + M_{\text{th}}, \qquad (2)$$
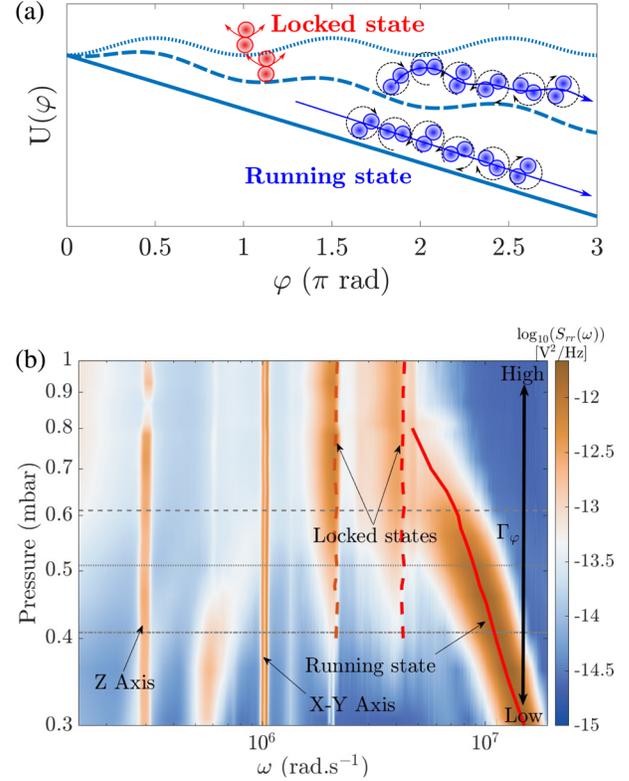
FIG. 1. (a) Illustration of the energy landscape for the rotation of the Brownian dimer around the optical axis for three different tilts. When the polarization is linear (blue dotted line), the potential is not tilted and the orientation of the dimer remains in the locked state. Conversely, for a circular polarization (solid blue line) the potential wells disappear. For elliptical polarization (dashed line), the rotational motion can change from a running state (spinning) to a locked state (torsional) and vice versa. (b) Surface plot in log-log scales of the angular vibration and translational power spectral densities as a function of the gas pressure for a beam ellipticity of $\phi_{\lambda/4} = 25°$ and an optical power of 180 mW. The solid and dashed curves (red) represent the local maxima of the PSD computed by Langevin simulations of Eq. (2). The three grey horizontal curves at 0.41 mbar, 0.51 mbar, and 0.61 mbar outline the two-state coexistence region where the middle line denotes the maximum of intermittency.

where Γ_φ is the rotational damping rate and $M_{\text{th}} = \sqrt{2k_BTI_\perp\Gamma_\varphi}\zeta(t)$ is the thermal torque with $\zeta(t)$ a Gaussian noise of zero mean value. M is given by Eq. (1).

Figure 1(b) shows the position and orientation power spectral densities as a function of pressure, along with the numerical Langevin simulations (solid red curves). For consistency, we also show the frequencies associated with translational motions in the X, Y, and Z directions that are independent of gas pressure. The observed nondegeneracy of the transverse frequencies X, Y is expected for a noncircularly polarized laser beam. In the high friction limit, the torsional dynamics dominate the dimer orientation motion and their resonance frequencies remain constant in relation to pressure. Conversely, the rotational

dynamics is dominant in the low friction regime, i.e., at low pressure, and its angular frequency, Ω_R, rises as the inverse of the gas damping.

The red solid curves in Fig. 1(b) show a good agreement between the experiment and one-dimensional simulations of Eq. (2). One can also clearly see that the bistability region is quantitatively well described by the model. The two locked states observed in the spectral densities are also found in the numerical simulations, and correspond to the fundamental peak and its overtone. Although not within the scope of this Letter, we do not preclude contributions with other angles leading to coupling with extra motional degrees of freedom. The experimental determination of the dimer size and shape by the calibration procedure [17] is used for calculating the moments of inertia and polarizabilities. The latter are further supported numerically using COMSOL MULTIPHYSICS. We find that $I_\perp = 2 \times 10^{-32}$ kg m^2, M_C and M_L are, respectively, of the order of 2×10^{-22} N m and 6×10^{-20} N m, in good agreement with both experimental and numerical results.

As mentioned above, in the calculation of optical torques the contribution of *scattering* is included in addition to the usual *extinction* contribution [41]. Since the polarization of the trapping beam is not linear, this scattering torque is crucial to reproduce quantitatively the experimental results, particularly when the dimer spins. In many previous works, the scattering torque was ignored because the rotational Langevin equation was only qualitatively discussed. It is worth noting that if the scattering torque is not taken into account, the particle's rotation speed is overestimated by typically an order of magnitude for the actual dimer [17] and much more for a spheroid (data not shown). Some quantitative deviations between theory and experiment appear at low pressure but without greatly affecting the giant diffusion effect.

We now consider the quantitative study of this stochastic nonequilibrium phenomenon. Figure 2 shows the time traces of the angular velocity $\dot\varphi$ obtained by short time Fourier transforms in the bistability region. In the locked state, the mean angular velocity is $\langle\dot\varphi\rangle_L \equiv 0$. While the mean rotational speed, $\langle\dot\varphi\rangle_R$, in the running state increases continuously with the pressure drop. The most noticeable feature of the time traces is the two-state noise-induced transitions, where the maximum of intermittency occurs in the middle of the bistability region at about $P \approx 0.56$ mbar [Fig. 1(b)].

We use the time traces of angular velocities to determine the mean occupation times in the locked and running states. Figure 3(a) shows the distributions $P(\tau/\langle\tau\rangle)$ of the mean occupation times, recorded for different gas pressures. These distributions decrease exponentially as expected for a Kramers-like problem. Deeper insight into two-state coexistence can be gained if we plot the pressure dependence of the average occupancy times in the locked and running states, as shown in Fig. 3(b), both for experimental
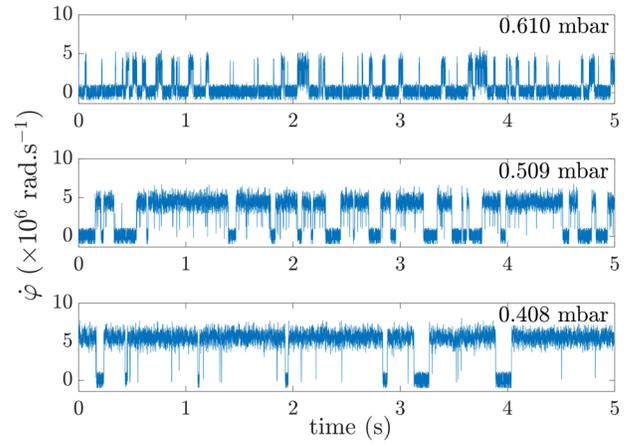
FIG. 2. Time traces of the dimer angular velocity $\dot\varphi$ obtained by short-time Fourier transform for the three pressures that are shown as gray horizontal curves in Fig. 1(b).

and numerical data. It can be evidenced that when $\Gamma_\varphi \ll \Omega_L$ (as in this case), the transition rate r_L out of a locked state (regardless of the final state, locked or running) is independent of the friction coefficient, i.e., of the pressure. This is in agreement with our observations [see Fig. 3(b) red squares and solid line]. Besides, this value is well approximated by the well-known Arrhenius law, $1/\tau_L = r_L \sim \Omega_L \exp(-E_b/k_B T)$, E_b being the barrier height given by the potential difference between a minimum and the lower neighboring maximum [42]. This offers insight into how a temperature change affects the stability of the torque state. A different behavior is observed for transitions from a running to a locked state for low damping and finite temperatures. This behavior is explained by the fact that the rate r_R is such that $1/\tau_R = r_R \sim \Gamma_\varphi \propto P$ [43]. Note that some differences occurring at low pressure can be observed
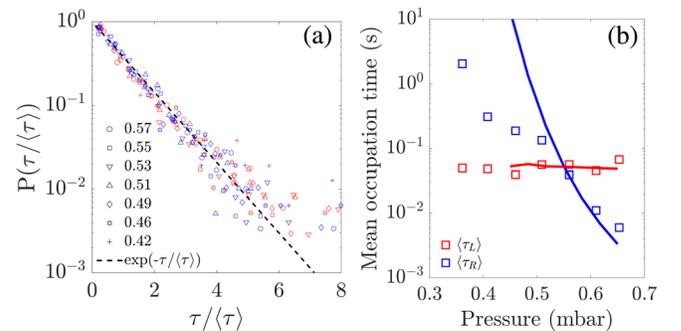
FIG. 3. (a) Probability distribution function of the occupation time from the locked to running states $P(\tau_L)$, red symbols, and the running to locked states $P(\tau_R)$, blue symbols, for various pressures where the bistability is observed. Exponential behaviors suggest that stochastic transitions between locked and running states are thermally activated, following an Arrhenius-type law. (b) Pressure dependence of the mean occupation times in the locked and running states [symbols: experiment, solid line: Langevin simulations, Eq. (2)].

between the one-dimensional model and the experiment [as seen in Fig. 3(b)]. They are not due to a time windowing effect, but could arise from the coupling between other rotational degrees of freedom, as seen below 0.45 mbar with the appearance of an additional resonance in the spectral densities [Fig. 1(b)].

In the rest of this Letter, we focus on the measurement of the effective rotational diffusion coefficient, which is defined by the Kubo relation

$$D_{\text{eff}} = \int_0^\infty dt' \langle [\dot{\varphi}(t') - \langle \dot{\varphi} \rangle][\dot{\varphi}(0) - \langle \dot{\varphi} \rangle] \rangle.$$

This coefficient satisfies the usual Einstein relation $\lim_{t \to \infty} \langle \varphi^2(t) \rangle - \langle \varphi(t) \rangle^2 = 2D_{\text{eff}}t$, where D_{eff} can in principle be enhanced by orders of magnitude over the free coefficient diffusion D_0 at the crossover from locked to running states. Interestingly, outside the region of bistability, the power spectral density of $\dot{\varphi}$ allows for a measurement of both $D_0 = k_B T / \Gamma_\varphi I_\perp$ and its related timescale $1/\Gamma_\varphi$. Surprisingly, we can derive a simple two-state stochastic noise model to fit our experimental results in the bistability region (see details in Sec. V.B of the Supplemental Material [17]). Since the parameter range we consider allows large timescale separations ($1/\Omega_R \ll 1/\Gamma_\varphi \ll \tau_L, \tau_R$), the spectral density of the rotation speed in the region of bistability reads

$$S_{\dot{\varphi}\dot{\varphi}}(\omega) = \frac{D_0}{1 + \frac{\omega^2}{\Gamma_\varphi^2}} + \frac{D_{\text{eff}}}{1 + \frac{\omega^2}{\Gamma_T^2}} \quad (3)$$

where $\Gamma_T = r_R + r_L$, is the total escape rate, corresponding to the longest timescale of the system. From the timetraces of the angular velocity $\dot{\varphi}$ (Fig. 2), we compute the power spectral densities of the rotation velocity (defined as the Fourier transform of the rotational velocity autocorrelation function) in the coexistence regime, as shown in Fig. 4(a). Using then Eq. (3), we can determine the effective diffusion D_{eff} relative to D_0, that is displayed in Fig. 4(b) as a function of pressure. Note that Γ_φ and Γ_T are also measured, allowing us to corroborate the values of the nanodimer size and its aspect ratio. To go further into the two-state model, we use the transition rates r_R and r_L deduced from Fig. 3 to calculate D_{eff}. In our parameter regime, the two-state model gives an expression that bears much similarities with those developed in [11,44–46]

$$D_{\text{eff}} = \langle \dot{\varphi} \rangle_R^2 \frac{r_L r_R}{(r_L + r_R)^3}, \quad (4)$$

where $\langle \dot{\varphi} \rangle_R$ is the average angular velocity taken only over the running states of the whole temporal trace. Comparison of the filled and open circles in Fig. 4(b) indicates that when Eq. (4) is used with the results obtained from occupancy times, good agreement is obtained with the diffusion
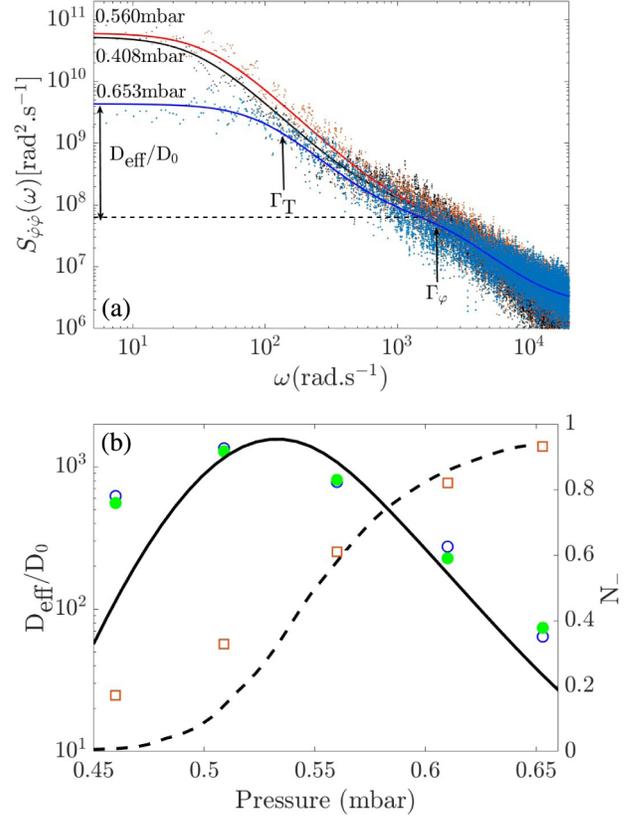
FIG. 4. (a) Measured power spectral densities of the dimer angular velocity (dots) and double Lorentzian fit [Eq. (3), solid curves] at the boundaries of the bistable region ($P = 0.653$ mbar in blue, $P = 0.408$ mbar in black), and at the pressure around which the maximum of giant diffusion exists ($P = 0.560$ mbar in red). The dashed line represents the free-space diffusion coefficient D_0 at $P = 0.653$ mbar, the double arrow displays the excess of diffusion D_{eff}/D_0, while both the total escape rate Γ_T and the rotational damping rate Γ_φ are marked by vertical arrows. (b) On the left axis. Pressure dependence of the effective diffusion coefficient D_{eff} in units of D_0 estimated by two methods: (i) data from Fig. 4(a) are fitted by using Eq. (3), blue open circles, while (ii) transition rates obtained from Fig. 3 are used to calculate D_{eff} from Eq. (4), green filled circles. The black solid line results from the Langevin simulations [Eq. (2)]. On the right axis. Proportion of the mean occupancy in the locked state (red squares: experiment and black dashed line: Langevin simulations).

estimate by spectral densities by using Eq. (3). The occupancy rate in the locked state defined as $N_- = \langle \tau_L \rangle / (\langle \tau_L \rangle + \langle \tau_R \rangle)$ is represented by red squares in Fig. 4(b). We observe that the giant increase in the effective diffusion coefficient is roughly maximal at a pressure where the states are evenly distributed.

In conclusion, we have observed in a very small pressure range a giant increase of the diffusion coefficient in the underdamped and weak noise limit. Carefully calculating the optical torque, a reasonable quantitative agreement has been obtained using a one-dimensional Langevin model. This supports evidence that even though the real system

dynamics has six dimensions, it can be reduced to a one-dimensional system within at least some parameter regimes. Cooling the translational (and possibly rotational) degrees of freedom would mitigate the rotranslational coupling [15,16], enabling ideally over a wide parameter regime to reach the true one-dimensional Brownian nano-rotor as described in Eq. (2). Thus, an optically levitated stator rotator constitutes an outstanding platform to study the issue of jump length distributions [47] and where its dynamics can be controlled down to the quantum ground state [48–50].

---

[*]louis.bellando.physique@gmail.com

[†]yacine.amarouchene@u-bordeaux.fr

[‡]mathias.perrin@u-bordeaux.fr

[§]yann.louyer@u-bordeaux.fr

[1] H. Kramers, Brownian motion in a field of force and the diffusion model of chemical reactions, Physica (Amsterdam) **7**, 284 (1940).

[2] H. Risken, *The Fokker-Planck Equation: Methods of Solution and Applications Second Edition* (Springer, New York, 1989).

[3] L. Longobardi, D. Massarotti, G. Rotoli, D. Stornaiuolo, G. Papari, A. Kawakami, G. P. Pepe, A. Barone, and F. Tafuri, Thermal hopping and retrapping of a brownian particle in the tilted periodic potential of a NbN/MgO/NbN Josephson junction, Phys. Rev. B **84**, 184504 (2011).

[4] R. Hayashi, K. Sasaki, S. Nakamura, S. Kudo, Y. Inoue, H. Noji, and K. Hayashi, Giant Acceleration of Diffusion Observed in a Single-Molecule Experiment on F1-ATPase, Phys. Rev. Lett. **114**, 248101 (2015).

[5] S. Strogatz, *Sync: The Emerging Science of Spontaneous Order* (Hyperion, New York, 2003).

[6] J. W. M. Frenken and J. F. van der Veen, Observation of Surface Melting, Phys. Rev. Lett. **54**, 134 (1985).

[7] S.-H. Lee and D. G. Grier, Giant Colloidal Diffusivity on Corrugated Optical Vortices, Phys. Rev. Lett. **96**, 190601 (2006).

[8] M. Evstigneev, O. Zvyagolskaya, S. Bleil, R. Eichhorn, C. Bechinger, and P. Reimann, Diffusion of colloidal particles in a tilted periodic potential: Theory versus experiment, Phys. Rev. E **77**, 041107 (2008).

[9] P. Reimann, C. Van den Broeck, H. Linke, P. Hänggi, J. M. Rubi, and A. Pérez-Madrid, Giant Acceleration of Free Diffusion by Use of Tilted Periodic Potentials, Phys. Rev. Lett. **87**, 010602 (2001).

[10] G. Costantini and F. Marchesoni, Threshold diffusion in a tilted washboard potential, Europhys. Lett. **48**, 491 (1999).

[11] B. Lindner and I. M. Sokolov, Giant diffusion of underdamped particles in a biased periodic potential, Phys. Rev. E **93**, 042106 (2016).

[12] Y. Amarouchene, M. Mangeat, B. V. Montes, L. Ondic, T. Guerin, D. S. Dean, and Y. Louyer, Nonequilibrium Dynamics Induced by Scattering Forces for Optically Trapped Nanoparticles in Strongly Inertial Regimes, Phys. Rev. Lett. **122**, 183901 (2019).

[13] M. Mangeat, Y. Amarouchene, Y. Louyer, T. Guerin, and D. S. Dean, Role of nonconservative scattering forces and damping on brownian particles in optical traps, Phys. Rev. E **99**, 052107 (2019).

[14] L. Rondin, J. Gieseler, F. Ricci, R. Quidant, C. Dellago, and L. Novotny, Direct measurement of kramers turnover with a levitated nanoparticle, Nat. Nanotechnol. **12**, 1130 (2017).

[15] J. Ahn, Z. Xu, J. Bang, Y.-H. Deng, T. M. Hoang, Q. Han, R.-M. Ma, and T. Li, Optically Levitated Nanodumbbell Torsion Balance and GHz Nanomechanical Rotor, Phys. Rev. Lett. **121**, 033603 (2018).

[16] R. Reimann, M. Doderer, E. Hebestreit, R. Diehl, M. Frimmer, D. Windey, F. Tebbenjohanns, and L. Novotny, GHz Rotation of an Optically Trapped Nanoparticle in Vacuum, Phys. Rev. Lett. **121**, 033602 (2018).

[17] See Supplemental Materials at http://link.aps.org/supplemental/10.1103/PhysRevLett.129.023602, which includes Refs. [18–32], for a complete description of our theoretical approach and the numerical methods used in the present paper. Detailed description of the experimental apparatus and also for the particle's size and shape caracterisation procedures are also provided.

[18] C. Van den Broeck, Taylor dispersion revisited, Physica (Amsterdam) **168A**, 677 (1990).

[19] L. Novotny and B. Hecht, *Principles of Nano-Optics* (Cambridge University Press, Cambridge, England, 2006).

[20] E. Hebestreit, M. Frimmer, R. Reimann, C. Dellago, F. Ricci, and L. Novotny, Calibration and energy measurement of optically levitated nanoparticle sensors, Rev. Sci. Instrum. **89**, 033111 (2018).

[21] P. V. Ruijgrok, N. R. Verhart, P. Zijlstra, A. L. Tchebotareva, and M. Orrit, Brownian Fluctuations and Heating of an Optically Aligned Gold Nanorod, Phys. Rev. Lett. **107**, 037401 (2011).

[22] J. Gieseler, R. Quidant, C. Dellago, and L. Novotny, Dynamic relaxation of a levitated nanoparticle from a non-equilibrium steady state, Nat. Nanotechnol. **9**, 358 (2014).

[23] A. Pinchuk and G. Schatz, Anisotropic polarizability tensor of a dimer of nanospheres in the vicinity of a plane substrate, Nanotechnology **16**, 2209 (2005).

[24] H. Rudolph, J. Schäfer, B. A. Stickler, and K. Hornberger, Theory of nanoparticle cooling by elliptic coherent scattering, Phys. Rev. A **103**, 043514 (2021).

[25] S. Albaladejo, R. Gómez-Medina, L. S. Froufe-Pérez, H. Marinchio, R. Carminati, J. F. Torrado, G. Armelles, A. García-Martín, and J. J. Sáenz, Radiative corrections to the polarizability tensor of an electrically small anisotropic dielectric particle, Opt. Express **18**, 3556 (2010).

[26] J. G. Kirkwood and J. Riseman, The intrinsic viscosities and diffusion constants of flexible macromolecules in solution, J. Chem. Phys. **16**, 565 (1948).

[27] B. Carrasco and J. Garcia de la Torre, Improved hydrodynamic interaction in macromolecular bead models, J. Chem. Phys. **111,** 4817 (1999).

[28] B. Dahneke, Viscous resistance of straight-chain aggregates of uniform spheres, Aerosol Sci. Technol. **1,** 179 (1982).

[29] R. A. Millikan, Coefficients of slip in gases and the law of reflection of molecules from the surfaces of solids and liquids, Phys. Rev. **21,** 217 (1923).

[30] J. Gieseler, L. Novotny, and R. Quidant, Thermal nonlinearities in a nanomechanical oscillator, Nat. Phys. **9,** 806 (2013); M. Yoneda and K. Aikawa, Thermal broadening of the power spectra of laser-trapped particles in vacuum, J. Phys. B **50,** 245501 (2017).

[31] J. Corson, G. W. Mulholland, and M. R. Zachariah, Calculating the rotational friction coefficient of fractal aerosol particles in the transition regime using extended kirkwood-riseman theory, Phys. Rev. E **96,** 013110 (2017).

[32] D. A. Sivak, J. D. Chodera, and G. E. Crooks, Time step rescaling recovers continuous-time dynamical properties for discrete-time langevin integration of nonequilibrium systems, J. Phys. Chem. B **118,** 6466 (2014).

[33] A. Ashkin and J. M. Dziedzic, Feedback stabilization of optically levitated particles, Appl. Phys. Lett. **30,** 202 (1977).

[34] D. Hümmer, R. Lampert, K. Kustura, P. Maurer, C. Gonzalez-Ballestero, and O. Romero-Isart, Acoustic and optical properties of a fast-spinning dielectric nanoparticle, Phys. Rev. B **101,** 205416 (2020).

[35] G. D. Bruce, P. Rodríguez-Sevilla, and K. Dholakia, Initiating revolutions for optical manipulation: the origins and applications of rotational dynamics of trapped particles, Adv. Phys. X **6,** 1838322 (2021).

[36] M. Rashid, M. Toroš, A. Setter, and H. Ulbricht, Precession Motion in Levitated Optomechanics, Phys. Rev. Lett. **121,** 253601 (2018).

[37] B. A. Stickler, K. Hornberger, and M. S. Kim, Quantum rotations of nanoparticles, Nat. Rev. Phys. **3,** 589 (2021).

[38] B. A. Stickler, B. Papendell, S. Kuhn, B. Schrinski, M. Millen, J. andArndt, and K. Hornberger, Probing macroscopic quantum superpositions with nanorotors, New J. Phys. **20,** 122001 (2018).

[39] J. Bang, T. Seberson, P. Ju, J. Ahn, Z. Xu, X. Gao, F. Robicheaux, and T. Li, Five-dimensional cooling and non-linear dynamics of an optically levitated nanodumbbell, Phys. Rev. Research **2,** 043054 (2020).

[40] Y. Arita, M. Mazilu, and K. Dholakia, Laser-induced rotation and cooling of a trapped microgyroscope in vacuum, Nat. Commun. **4,** 2374 (2013).

[41] M. Nieto-Vesperinas, Optical torque: Electromagnetic spin and orbital-angular-momentum conservation laws and their significance, Phys. Rev. A **92,** 043843 (2015).

[42] M. Büttiker and R. Landauer, Escape-energy distribution for particles in an extremely underdamped potential well, Phys. Rev. B **30,** 1551 (1984).

[43] M. Büttiker, E. P. Harris, and R. Landauer, Thermal activation in extremely underdamped Josephson-junction circuits, Phys. Rev. B **28,** 1268 (1983).

[44] S. Machlup, Noise in semiconductors: Spectrum of a two-parameter random signal, J. Appl. Phys. **25,** 341 (1954).

[45] P. K. Ghosh, P. Hänggi, F. Marchesoni, F. Nori, and G. Schmid, Brownian transport in corrugated channels with inertia, Phys. Rev. E **86,** 021112 (2012).

[46] C. W. Gardiner, *Handbook of Stochastic Methods for Physics, Chemistry and the Natural Sciences,* 3rd ed., Springer Series in Synergetics Vol. 13 (Springer-Verlag, Berlin, 2004), pp. xviii+415.

[47] M. Borromeo, G. Costantini, and F. Marchesoni, Critical Hysteresis in a Tilted Washboard Potential, Phys. Rev. Lett. **82,** 2820 (1999).

[48] U. Delic, M. Reisenbauer, K. Dare, D. Grass, V. Vuletic, N. Kiesel, and M. Aspelmeyer, Cooling of a levitated nanoparticle to the motional quantum ground state, Science **367,** 892 (2020).

[49] L. Magrini, P. Rosenzweig, C. Bach, A. Deutschmann-Olek, S. G. Hofer, S. Hong, N. Kiesel, A. Kugi, and M. Aspelmeyer, Real-time optimal quantum control of mechanical motion at room temperature, Nature (London) **595,** 373 (2021).

[50] F. Tebbenjohanns, M. L. Mattana, M. Rossi, M. Frimmer, and L. Novotny, Quantum control of a nanoparticle optically levitated in cryogenic free space, Nature (London) **595,** 378 (2021).